Target Sidelobes Removal via Sparse Recovery in the Subband Domain of an OFDM RadCom System

Stéphanie Bidon*, Damien Roque* and Steven Mercier*
*ISAE-SUPAERO, Université de Toulouse, France
Email: {stephanie.bidon,damien.roque,steven.mercier}@isae-supaero.fr

***Abstract*—In this paper, the problem of target masking induced by sidelobes arising in an OFDM RadCom System is considered. To fully exploit the waveform structure and address practical scenarios, we propose to deal with the sidelobes in the subband domain via sparse recovery. Accordingly, we design a sparsifying dictionary modeling at the same time the target's peak *and* pedestal. Results on synthetic data show that our approach allows one to remove not only the target random sidelobes but also range ambiguities arising when all subbands are not active.**

I. Introduction

In radar/communication waveform sharing scenarios, multicarrier modulations are usually a good choice because of their robustness against time-frequency selective channels [1]. For example, the cyclic prefixed orthogonal frequency division multiplexing (CP-OFDM) waveform has been proposed to diagonalize frequency-selective channels, at the expense of spectral efficiency loss incurred by the CP [2]. Its low-complexity implementation and its adoption in various communication standards (*e.g.*, DVB-T, LTE) made it attractive in both active and passive radar applications [3]–[5].

In particular, the so-called "symbol-based" radar receiver initially proposed in a monostatic scenario in [6], [7] transforms in a first stage the received signal in the "subband" domain via a linear multicarrier receiver. After a symbol removal step, the range-Doppler map is directly obtained through a two-dimensional discrete Fourier transform (2D-DFT). As for correlation-based techniques [5], the subband approach generates self-interference in the range-Doppler map; the latter is however characterized not only by a pedestal (also referred to as random sidelobes) but also by a target peak loss [8].

If self-interference can be handled on receive in the fast-time/slow-time domain (*e.g.,* extensive cancellation algorithm in [9], CLEAN-based technique in [10]), operating in the subband/slow-time domain has several merits. For example, pilots can be easily discarded to avoid ghosting [5]. Additionally, zero-Doppler clutter can be effectively rejected at the output of a CP-OFDM receiver, assuming a long enough cyclic prefix [11]. In multiuser scenarios with per-subcarrier resources allocation (*e.g.*, LTE, 5G-NR) [12], [13], it is also reasonable to remove contribution from other users at the early stages of the receiver.

The work of Steven Mercier is supported by DGA/MRIS under grant 2017.60.0005 and Thales DMS.

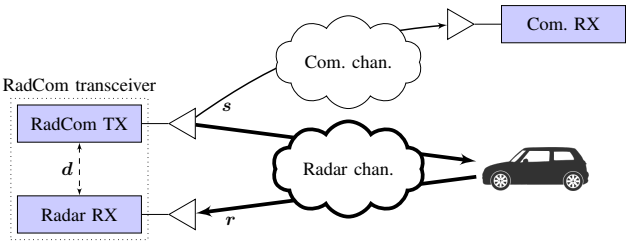

Fig. 1. Illustration of a typical RadCom scenario. Transmitted symbols are known by the radar receiver.

In this paper, we consider a RadCom scenario as depicted in Fig. 1 (also known as monostatic broadcast channel [14]) and propose to remove the target self-interference in the subband/slow-time domain. Accordingly, we first show that using a sparse signal representation (SSR) with an adequate dictionary allows the targets pedestal to be removed while recovering full gain on their peak. We then illustrate that the SSR technique expressed in the subband domain is also able to leverage range ambiguities arising when all subbands are not available to the user.

The paper is organized as follows. Section II describes the multicarrier transmitted signal, the multitarget channel model and the observation in the subband domain. Section III recalls a Bayesian sparse reconstruction method for targets estimation in presence of self-interference. Section IV discusses the performance of the proposed approach. Finally, conclusions and perspectives are given in Section V.

Notation: $\mathcal{I}_N$ is the integer sequence $\{0,\dots,N-1\}$. Matrices (resp. vectors) are represented by uppercase (resp. lowercase) italic bold letters. $\boldsymbol{I}$ and $\boldsymbol{0}$ are the identity and null matrices, $[\boldsymbol{A}]_{m,n}$ denotes the element in the mth row and nth column of $\boldsymbol{A}$. $\cdot^T$, $\cdot^*$ and $\cdot^H$ refer to transpose, conjugate and conjugate transpose. $\otimes$ denotes the Kronecker product, $\delta_{\cdot,\cdot}$ is the Kronecker symbol and $\delta()$ is the Dirac delta function.

II. Linear multicarrier system over a multitarget radar channel

In this Section, we describe the radar system depicted in Fig. 2.

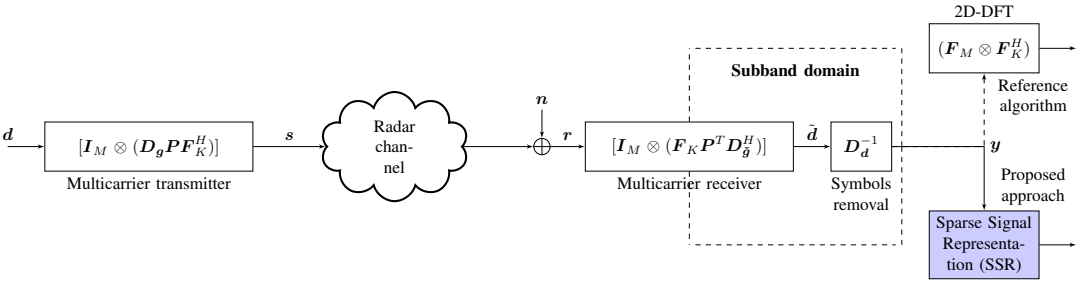

Fig. 2. Block diagram of the proposed multicarrier radar system.

A. Multicarrier transmitter

Let us consider a multicarrier signal composed of K subcarriers and M blocks (*i.e.,* sweeps). Symbols $d_{k,m}$, $(k,m) \in \mathcal{I}_K \times \mathcal{I}_M$ can be data or pilot elements, taken in potentially different constellations (*e.g.*, phase-shift keying). Each $d_{k,m}$ is pulse-shaped by $g_{k,m}(t) \triangleq g(t - mT_0)\exp(j2\pi kF_0 t)$ with $g(t)$ a generator function with support $[0; T_0)$ and T_0, F_0 elementary spacing between symbols in time and frequency, respectively. In other words, T_0 is the sweep repetition interval. In the usual CP-OFDM case, $g(t)$ is constant over its support, however there exists various alternatives, potentially non-rectangular [15], [16]. If K is large enough, the occupied bandwidth of the transmitted signal can be approximated by KF_0; the critically sampled multicarrier signal is given by [17]

$$\boldsymbol{s} = \left[\boldsymbol{I}_M \otimes (\boldsymbol{D_g P F}_K^H)\right] \boldsymbol{d} \tag{1}$$

with

- $\boldsymbol{d}$ the symbol vector with $[\boldsymbol{d}]_{k+mK} \triangleq d_{k,m}$;
- $\boldsymbol{F}_K$ the unitary K-by-K DFT matrix;
- $\boldsymbol{P}$ the L-by-K cyclic extension matrix with $L \triangleq T_0F_0K \geq K$ and entries $[\boldsymbol{P}]_{l,k} \triangleq \delta_{l,k} + \delta_{l,k+K}$;
- $\boldsymbol{D_g}$ is the L-by-L weighting matrix defined by $\boldsymbol{D_g} \triangleq \mathrm{diag}\{\boldsymbol{g}\}$ with $[\boldsymbol{g}]_l \triangleq g[l] = g(l/(KF_0))$, $l \in \mathcal{I}_L$ the critically sampled version of the generator function with, by convention, $\|\boldsymbol{g}\|_2^2 = K$.

B. Multitarget radar channel

The radar channel consists of N targets, considered as single point scatterers (presence of clutter is not considered within this work). Each target n respects the following assumptions:

- constant complex amplitude α_n during the coherent processing interval MT_0 (*i.e.*, duration of the transmitted signal);
- unambiguous range $R_{0,n} \leq (K-1)\Delta_R$ with $\Delta_R = c/(2KF_0)$ the range resolution and c the speed of light;
- Doppler-induced frequency-shift $F_{d,n} = 2v_nF_c/c \ll KF_0$ with v_n the radial velocity of the target, F_c the carrier frequency.

The latter assumption justifies a critical sampling of the received signal at rate KF_0. Without loss of generality, we assume integer range gates $l_{0,n} \triangleq R_{0,n}/\Delta_R$ such that the discrete-time received signal can be expressed as

$$\boldsymbol{r} = \sum_{n=0}^{N-1} \alpha_n \boldsymbol{Z}_n \boldsymbol{s} + \boldsymbol{n} \tag{2}$$

where $[\boldsymbol{Z}_n]_{(l,l')\in\mathcal{I}_{LM}\times\mathcal{I}_{LM}} \triangleq e^{j2\pi f_{d,n}l/L}\delta_{l,l'+l_{0,n}}$ is the range-Doppler shift matrix related to the nth target, $f_{d,n} = F_{d,n}T_0$ is its normalized Doppler shift and $\boldsymbol{n}$ is the thermal noise assumed white and Gaussian with power σ^2, *i.e.,* $\boldsymbol{n} \sim \mathcal{CN}\left(\boldsymbol{0}, \sigma^2\boldsymbol{I}\right)$.

C. Multicarrier receiver, symbols removal

As proposed in [6], the received signal $\boldsymbol{r}$ is projected in the subband domain thanks to a linear multicarrier receiver

$$\tilde{\boldsymbol{d}} = [\boldsymbol{I}_M \otimes (\boldsymbol{F}_K \boldsymbol{P}^T \boldsymbol{D}_{\check{\boldsymbol{g}}}^H)]\boldsymbol{r} \tag{3}$$

where $\boldsymbol{D}_{\check{\boldsymbol{g}}} \triangleq \mathrm{diag}\{\check{\boldsymbol{g}}\}$ and $\check{\boldsymbol{g}}$ is the L-length received pulse vector. The latter is defined under a (bi)orthogonality constraint with respect to the transmitter, namely $\boldsymbol{P}^T\boldsymbol{D}_{\check{\boldsymbol{g}}}^H\boldsymbol{D_g P} = \boldsymbol{I}_K$. For the particular case of CP-OFDM, expressions of $\boldsymbol{g}, \check{\boldsymbol{g}}$ are given in (17); it follows that $\boldsymbol{P}^T\boldsymbol{D}_{\check{\boldsymbol{g}}}^H$ removes the CP of each block. An element-wise symbols removal w.r.t. the initial mapping (1) is argued for steering vectors reconstruction if $f_{d,n} \to 0$ and $l_{0,n} \leq L - K$ [6]:

$$\boldsymbol{y} = \boldsymbol{D}_{\boldsymbol{d}}^{-1}\tilde{\boldsymbol{d}} \quad \text{with} \quad \boldsymbol{D}_{\boldsymbol{d}}^{-1} \triangleq \mathrm{diag}^{-1}(\boldsymbol{d}) \tag{4}$$

As per [8], the signal $\boldsymbol{y}$ can be split into three main terms

$$\boldsymbol{y} = \underbrace{\boldsymbol{y}^{(t)} + \boldsymbol{y}^{(i)}}_{\text{targets}} + \boldsymbol{y}^{(n)}$$

with

$$\boldsymbol{y}^{(t)} = \sum_{n=0}^{N-1} \alpha_n A_{\check{g},g}(l_{0,n}; f_{d,n}/L)\boldsymbol{e}_d(f_{d,n}) \otimes \boldsymbol{e}_r(l_{0,n}) \tag{5}$$

$$A_{\check{g},g}(l_0; f_d) \triangleq \frac{1}{K}\sum_{l=-\infty}^{+\infty} \check{g}^*[l]g[l-l_0]e^{j2\pi f_d l} \tag{6}$$

$$[\boldsymbol{e}_r(l_{0,n})]_k \triangleq \exp(-j2\pi l_{0,n}k/K) \quad k \in \mathcal{I}_K \tag{7}$$

$$[\boldsymbol{e}_d(f_{d,n})]_m \triangleq \exp(j2\pi f_{d,n}m) \quad m \in \mathcal{I}_M \tag{8}$$

$$\boldsymbol{y}^{(n)} = \boldsymbol{D}_{\boldsymbol{d}}^{-1}[\boldsymbol{I}_M \otimes (\boldsymbol{F}_K \boldsymbol{P}^T \boldsymbol{D}_{\check{\boldsymbol{g}}}^H)]\boldsymbol{n} \tag{9}$$

where

- $\boldsymbol{y}^{(t)}$ is the usual component associated with the targets peak; it does not depend on the data symbols but

on the targets' range and Doppler steering vectors $\boldsymbol{e}_r$, $\boldsymbol{e}_d$ and on the cross-ambiguity function $A_{\check{g},g}$ that induces a range-Doppler dependent loss on the peaks.

$\boldsymbol{y}^{(i)}$ is the targets pedestal component that strongly depends on 1) the target range-Doppler location and amplitude; 2) the data symbols. Its expression is not recalled here for conciseness [8]. This component can be considered as a random variable, shown to be white with power σ_i^2 in the range-Doppler map (if symbols are zero-mean, independent and identically distributed and taken in proper constellations) [8]. Hereafter, we will rather consider the pedestal component, namely the so-called random sidelobes, as deterministic (cf. Sec. III).

$\boldsymbol{y}^{(n)}$ is the noise contribution after symbols removal; its power σ_n^2 has a simple expression given in [8].

D. Reference algorithm: 2D-DFT

When the pedestal component $\boldsymbol{y}^{(i)}$ can be neglected (*e.g.*, targets with round-trip delays shorter than the CP and very low Doppler), a simple two-dimensional discrete Fourier transform can be used to compute the range-Doppler map, as initially proposed in [6]

$$\boldsymbol{x} = (\boldsymbol{F}_M \otimes \boldsymbol{F}_K^H)\boldsymbol{y}. \tag{10}$$

In the following, we focus on the case where $\boldsymbol{y}^{(i)}$ is significant (*e.g.*, powerful targets with high range and/or Doppler), potentially creating target masking issues in the range-Doppler map obtained from (10).

III. Sparse Bayesian estimation in the subband domain

In this Section, we propose to use an SSR approach in the subband domain to estimate the targets while offsetting the self-interference phenomenon.

A. Sparse observation model

Using (2)-(3)-(4), the signal received after symbol removal can be rewritten in the subband/slow-time domain as

$$\boldsymbol{y} = \underbrace{\sum_{n=0}^{N-1} \alpha_n \boldsymbol{h}_n}_{\text{targets}} + \boldsymbol{y}^{(n)} \tag{11}$$

where $\boldsymbol{h}_n$ is the steering vector of the nth target; it enjoys an efficient FFT-based implementation, *i.e.*,

$$\boldsymbol{h}_n = \boldsymbol{D}_{\boldsymbol{d}}^{-1}[\boldsymbol{I}_M \otimes (\boldsymbol{F}_K \boldsymbol{P}^T \boldsymbol{D}_{\check{\boldsymbol{g}}}^H)]\boldsymbol{Z}_n \boldsymbol{s}. \tag{12}$$

It is worth noticing that the steering vector (12) entails at the same time the target's peak component *and* its pedestal. This is a major difference compared to sparse techniques previously described, *e.g.,* [18].

Given (11), a natural sparsifying dictionary can be built by 1) discretizing the range-Doppler domain; 2) concatenating the steering vectors of the form (12) associated with each range-Doppler bin created. The sparse observation model obtained is thus

$$\boldsymbol{y} = \boldsymbol{H}\boldsymbol{\alpha} + \boldsymbol{y}^{(n)} \tag{13}$$

where

$\boldsymbol{H}$ is a $KM \times \bar{K}\bar{M}$ dictionary with $\bar{K}, \bar{M}$ the number of bins in the range and Doppler domains, respectively;

$\boldsymbol{\alpha}$ is the target amplitude vector in the reconstructed range-Doppler domain.

The $\bar{i}$th column of $\boldsymbol{H}$ is

$$\boldsymbol{h}_{\bar{i}} \triangleq \boldsymbol{D}_{\boldsymbol{d}}^{-1}[\boldsymbol{I}_M \otimes (\boldsymbol{F}_K \boldsymbol{P}^T \boldsymbol{D}_{\check{\boldsymbol{g}}}^H)]\boldsymbol{Z}_{\bar{i}} \boldsymbol{s}$$

where $\boldsymbol{Z}_{\bar{i}}$ is the range-Doppler shift matrix introduced in (2) with range gate $l_0 = \bar{k}K/\bar{K}$ and normalized Doppler frequency $f_d = \bar{m}/\bar{M}$ where $\bar{i} = \bar{k} + \bar{m}\bar{K}$.

The parameter of interest to be estimated in (13) is the amplitude vector $\boldsymbol{\alpha}$. To reflect the sparsity of the target scene and since the problem of estimation can be ill-posed (if $\bar{M}\bar{K} > KM$), additional constraints should be added to (13). To that end, we choose the Bayesian philosophy though other SSR techniques could be used.

B. Bayesian estimation

In this work, we use a previously described algorithm [19]. Its basic principle is recalled in the next two sections.

1) Prior model: In a Bayesian framework, unknown parameters are considered as random and are assigned a prior probability density function (pdf). It is chosen to convey relevant information about the parameters and must ensure at the same time some degree of mathematical tractability. The latter issue is usually addressed by choosing conjugate priors [20] whereas the former is addressed by modeling and/or selecting appropriately the parameters of the prior pdfs.

A hierarchical Bayesian model is thus designed in [19] as follows

$$\pi(\alpha_{\bar{i}}|w, \sigma_\alpha^2) = (1-w)\delta(\alpha_{\bar{i}}) + w\, \mathcal{CN}\left(\alpha_{\bar{i}}|0, \sigma_\alpha^2\right) \tag{14a}$$

$$\pi(w) = \mathbb{I}_{[0,1]}(w) \tag{14b}$$

$$\pi(\sigma_\alpha^2) = \mathcal{IG}\left(\sigma_\alpha^2|\beta_0, \beta_1\right) \propto \frac{e^{-\beta_1/\sigma_\alpha^2}}{{\sigma_\alpha^2}^{\beta_0+1}} \mathbb{I}_{\mathbb{R}_+^*}(\sigma_\alpha^2) \tag{14c}$$

$$\pi(\sigma_n^2) = \mathcal{IG}\left(\sigma_n^2|\gamma_0, \gamma_1\right) \propto \frac{e^{-\gamma_1/\sigma_n^2}}{{\sigma_n^2}^{\gamma_0+1}} \mathbb{I}_{\mathbb{R}_+^*}(\sigma_n^2) \tag{14d}$$

where $\propto$ means proportional to. In plain English (14a) means that a target is *a priori* present in each range-Doppler bin $\bar{i}$ with a probability w and its amplitude $\alpha_{\bar{i}}$ is Gaussian distributed with power σ_α^2. Since the target power can greatly vary within a target scene, σ_α^2 is itself assumed random with an inverse Gamma distribution (14c). This leads to a heavy tailed distribution thereby robustifying the prior model of $\alpha_{\bar{i}}$. In addition, the density of the target scene is unknown so that w is assumed uniformly distributed (14b). Finally, if the noise power σ_n^2 is not exactly known, it can be jointly estimated with the target scene assuming *a priori* an inverse Gamma distribution (14d).

In the model (14), the hyperparameters linked to the scale and shape parameters of the inverse Gamma distributions (14c)-(14d), namely (β_0, β_1) and (γ_0, γ_1), are numerically selected by the radar operator so as to give weight to the most probable values of σ_α^2 and σ_n^2 (cf. Sec. IV).

2) Estimation algorithm: According to the fully Bayesian model (13)-(14), the joint posterior distribution is expressed via Bayes theorem as

$$f(\boldsymbol{\alpha}, w, \sigma_\alpha^2, \sigma_n^2, |\boldsymbol{y}) \propto f(\boldsymbol{y}|\boldsymbol{\alpha}, \sigma_\alpha^2) \quad \text{(likelihood)}$$
$$\times \pi(\boldsymbol{\alpha}|w, \sigma_\alpha^2)\pi(w)\pi(\sigma_\alpha^2)\pi(\sigma_n^2) \quad \text{(priors)}.$$

Posterior distributions of each parameter $\zeta \in \boldsymbol{\theta}$, with $\boldsymbol{\theta} \triangleq \{\boldsymbol{\alpha}, w, \sigma_\alpha^2, \sigma_n^2\}$, cannot be easily manipulated so that a numerical alternative is chosen in [19]. The proposed estimation algorithm is a Monte-Carlo Markov Chain method that iteratively draws samples according to each full conditional, *viz*

$$\pi(\alpha_{\bar{i}}|\boldsymbol{y}, \boldsymbol{\theta}_{-\alpha_{\bar{i}}}) = (1 - w_{\bar{i}})\delta(\alpha_{\bar{i}}) + w_{\bar{i}}\, \mathcal{CN}\left(\alpha_{\bar{i}}|\mu_{\bar{i}}, \eta_{\bar{i}}^2\right) \quad (15a)$$
$$\pi(w|\boldsymbol{y}, \boldsymbol{\theta}_{-w}) = \mathcal{B}e\left(w|1 + \|\boldsymbol{\alpha}\|_0, 1 + \bar{K}\bar{M} - \|\boldsymbol{\alpha}\|_0\right) \quad (15b)$$
$$\pi(\sigma_\alpha^2|\boldsymbol{y}, \boldsymbol{\theta}_{-\sigma_\alpha^2}) = \mathcal{IG}\left(\sigma_\alpha^2|\, \|\boldsymbol{\alpha}\|_0 + \beta_0, \|\boldsymbol{\alpha}\|_2^2 + \beta_1\right) \quad (15c)$$
$$\pi(\sigma_n^2|\boldsymbol{y}, \boldsymbol{\theta}_{-\sigma_n^2}) = \mathcal{IG}\left(\sigma_n^2|KM + \gamma_0, \|\boldsymbol{y} - \boldsymbol{H}\boldsymbol{\alpha}\|_2^2 + \gamma_1\right) \quad (15d)$$

where $\boldsymbol{\theta}_{-\zeta} = \boldsymbol{\theta}\backslash\{\zeta\}$, $\|\|_0$ is the number of nonzero elements in a vector, $\mathcal{B}e\,(|,)$ is the Beta pdf and the parameters in (15a) are

$$w_{\bar{i}} = \left[\frac{1-w}{w}\frac{\sigma_\alpha^2}{\eta_{\bar{i}}^2}\exp\left\{-\frac{|\mu_{\bar{i}}|^2}{\eta_{\bar{i}}^2}\right\} + 1\right]^{-1} \quad (16a)$$
$$\eta_{\bar{i}}^2 = \left\{\frac{1}{\sigma_\alpha^2} + \frac{\|\boldsymbol{h}_{\bar{i}}\|_2^2}{\sigma_n^2}\right\}^{-1} \quad (16b)$$
$$\mu_{\bar{i}} = \frac{\eta_{\bar{i}}^2}{\sigma_n^2}\boldsymbol{h}_{\bar{i}}^H \boldsymbol{e}_{\bar{i}} \quad (16c)$$

with $\boldsymbol{e}_{\bar{i}} = \boldsymbol{y} - \sum_{\bar{j}\neq\bar{i}} \alpha_{\bar{j}}\boldsymbol{h}_{\bar{j}}$.

Interestingly, the vector $\boldsymbol{e}_{\bar{i}}$ in (16c) represents the observation vector $\boldsymbol{y}$ in the subband/slow-time domain to which all the target components have been removed except that of the $\bar{i}$th range-Doppler bin. The amplitude $\alpha_{\bar{i}}$ is thus sampled in (15a) after rejecting all other target signatures, including their pedestal.

After a given number N_{bi} of iterations, the sampler (15) gives samples actually distributed according to their posterior distribution. Classical Bayesian estimators can be then numerically evaluated, particularly the minimum mean square error (MMSE) estimator of any parameter ζ in $\boldsymbol{\theta}$ is obtained as an empirical mean, *i.e.*,

$$\hat{\zeta}_{\text{mmse}} = N_r^{-1}\sum_{t=1}^{N_r}\zeta^{(t+N_{bi})}$$

where N_r is a sufficient number of samples.

IV. Numerical results

A. Scenario

Performance of the proposed strategy is assessed on synthetic data which are generated according to the model (2).

TABLE I
Target scene

n	0	1	2
Range bin $l_{0,n}$	5	10	25
Doppler bin $f_{d,n}M$; Doppler freq. (f_d)	7;(0.44)	0;(0)	7;(0.44)
SNR_{th}	15	17	35
Peak loss $A_{\check{g},g}(l_0; f_d)$ (dB)	-2.4	-1.8	-9.5
Random sidelobes power σ_i^2 (dB)	-15.8	-14.8	7.4

Symbols are generated as independent and uniformly distributed elements in a quadrature phase-shift keying (QPSK) constellation; they are thus zero-mean and assumed with unit variance. A conventional CP-OFDM waveform is considered by setting

$$g[l] = \begin{cases}\sqrt{K/L} & \text{if } 0 \le l \le L-1,\\ 0 & \text{otherwise,}\end{cases} \quad (17a)$$

$$\check{g}[l] = \begin{cases}0 & \text{if } 0 \le l \le L-K-1,\\ \sqrt{L/K} & \text{if } L-K \le l \le L-1,\\ 0 & \text{otherwise.}\end{cases} \quad (17b)$$

The target scene is described in Table I. In absence of self-interference, the postprocessing signal-to-noise-ratio (SNR) of a target is equal to [8]

$$\text{SNR}_{\text{th}} = \frac{\mathcal{E}\left\{|\alpha|^2\right\}K^2M}{\sigma^2\,\|\check{\boldsymbol{g}}\|_2^2}. \quad (18)$$

The SNR observed at the output of the 2D-DFT receiver (10) is in practice lower due to both the loss on the peak and the induced pedestal. Theoretical expressions can be found accordingly in [8].

B. Results with all subbands active

Typical range-Doppler maps obtained from the 2D-DFT (10) and the proposed SSR-based strategy are depicted in Fig. 3. As expected in the former approach, the strong target with high range and Doppler produces a high pedestal that hides the weakest ones. It is the sole target that can be clearly distinguished in Fig. 3a. On the contrary, with the proposed approach (cf. Fig.3b), each target can be recovered with its actual SNR (18). The dynamic range of the target scene is hence restored. Empirical posterior distributions obtained from the sampler (15) are also depicted in Fig. 4 and show rather peaked pdfs around each theoretical value despite moderately informative priors.

C. Results with only part of subbands active

In realistic scenarios, some subbands may not be used by the RadCom transceiver (*e.g.,* multiuser scenarios with per-subcarrier resources allocation). In that case on receive, the dimension of the observation $\boldsymbol{y}$ in (11) is accordingly reduced to the number of subbands $K_{\text{user}} < K$ exploited. Obviously, the actual target SNR (18) is thus diminished by a factor K_{user}/K. In addition given (5), using less subcarriers results for the target peak component in either range ambiguities and/or range resolution loss as dictated by the pattern of active

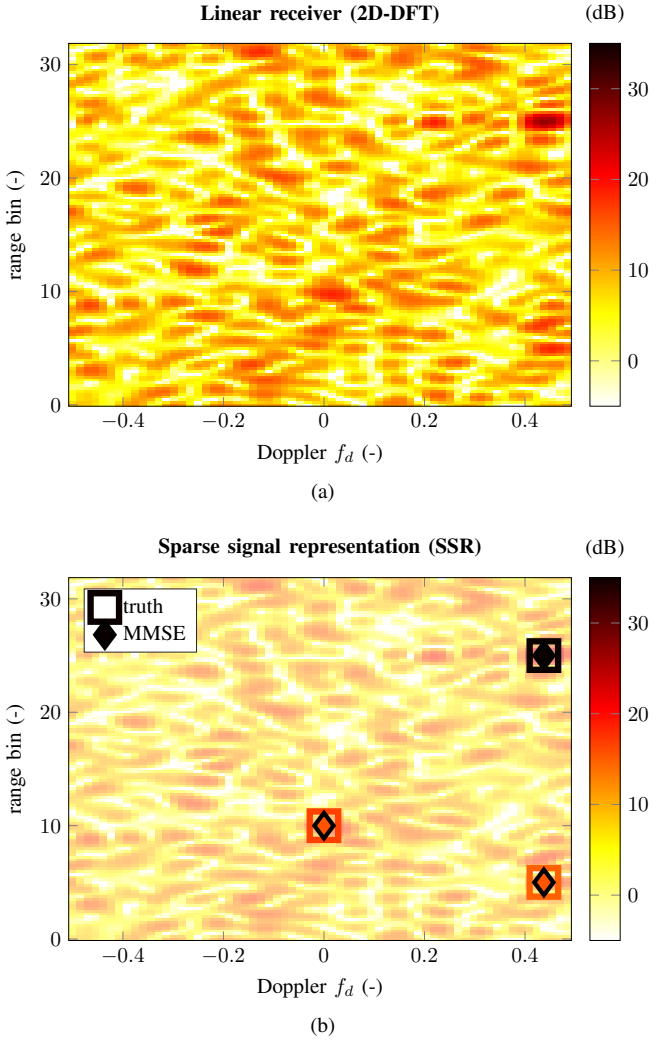

Fig. 3. Range-Doppler map with a CP-OFDM waveform. QPSK symbols, $M = 16$, $K = 32$, $L = 36$ (*i.e.,* $L/K = 1.125$), $\sigma^2 = 1$ (*i.e.,* $\sigma_n^2 = 1.125$), target parameters are described in Table I. (a) 2D-DFT output $|\boldsymbol{x}|$ (10). (b) Proposed SSR-based strategy output $K^2M/(\sigma^2\,\|\breve{\boldsymbol{g}}\|_2^2) \times |\hat{\boldsymbol{\alpha}}_{\text{mmse}}|^2$ (2D-DFT output depicted in transparent background as a reference): $\bar{K} = K$, $\bar{M} = M$, $(\beta_0, \beta_1) \approx (3, 50)$, $(\gamma_0, \gamma_1) \approx (2, 4)$, $(N_{bi}, N_r) = (200, 500)$.

subcarriers. As an example, we consider the case where one-in-two subbands are actually transmitting. As can be seen in Fig. 5a, this specific pattern leads to a pure range aliasing of the target peaks. Though still, the SSR technique is able to recover and disambiguate the target scene (cf. Fig. 5b). Indeed, contrary to the target peak component (5) the pedestal component $\boldsymbol{y}^{(i)}$ does not become range ambiguous with less subcarriers. Since the sparsifying dictionary is built on steering vectors (12) that entail the target pedestal signature, range ambiguity can be alleviated via SSR.

V. Conclusions and Future Work

In this work, we have proposed a strategy to estimate the target scene illuminated by an OFDM waveform. Particularly, a sparse representation technique is advocated for in the subband domain. Most importantly, the sparsifying dictionary is designed to model both the target's peak *and* pedestal. The proposed sparse recovery removes efficiently the traditional random sidelobes while preserving the gain on the target peak. In addition, working in the subband domain has several merits including the possibility to address a multiuser RadCom scenario. Interestingly, range ambiguities arising then are leveraged by the sparse recovery owing to the non-ambiguous nature of the pedestal signature. In future work, the presence of diffuse clutter should be dealt with too.

References

[1] P. Jung, "Pulse shaping, localization and the approximate eigenstructure of LTV channels (special paper)," in *2008 IEEE Wireless Communications and Networking Conference*, March 2008, pp. 1114–1119.

[2] Z. Wang and G. B. Giannakis, "Wireless multicarrier communications," *IEEE Signal Processing Magazine*, vol. 17, no. 3, pp. 29–48, May 2000.

[3] Y. L. Sit, L. Reichardt, C. Sturm, and T. Zwick, "Extension of the OFDM joint radar-communication system for a multipath, multiuser scenario," in *2011 IEEE RadarCon (RADAR)*, May 2011, pp. 718–723.

[4] R. F. Tigrek, W. J. A. D. Heij, and P. V. Genderen, "OFDM signals as the radar waveform to solve Doppler ambiguity," *IEEE Trans. Aerosp. Electron. Syst.*, vol. 48, no. 1, pp. 130–143, Jan 2012.

[5] J. E. Palmer, H. A. Harms, S. J. Searle, and L. Davis, "DVB-T passive radar signal processing," *IEEE Trans. Signal Process.*, vol. 61, no. 8, pp. 2116–2126, April 2013.

[6] C. Sturm, T. Zwick, and W. Wiesbeck, "An OFDM system concept for joint radar and communications operations," in *Veh. Tech. Conf., VTC Spring*, April 2009, pp. 1–5.

[7] C. Sturm and W. Wiesbeck, "Waveform design and signal processing aspects for fusion of wireless communications and radar sensing," *Proc. IEEE*, vol. 99, no. 7, pp. 1236–1259, July 2011.

[8] S. Mercier, D. Roque, and S. Bidon, "Study of the target self-interference in a low-complexity OFDM-based radar receiver," *IEEE Trans. Aerosp. Electron. Syst.*, pp. 1–1, 2018.

[9] F. Colone, D. W. O'Hagan, P. Lombardo, and C. J. Baker, "A multistage processing algorithm for disturbance removal and target detection in passive bistatic radar," *IEEE Trans. Aerosp. Electron. Syst.*, vol. 45, no. 2, pp. 698–722, April 2009.

[10] S. Mercier, D. Roque, and S. Bidon, "Successive self-interference cancellation in a low-complexity WCP-OFDM radar receiver," in *Proc. IEEE Asilomar Conf. Signals, Syst. Comput.*, Oct. 2018.

[11] Z. Zhao, X. Wan, Q. Shao, Z. Gong, and F. Cheng, "Multipath clutter rejection for digital radio mondiale-based HF passive bistatic radar with OFDM waveform," *IET Radar, Sonar Navigation*, vol. 6, no. 9, pp. 867–872, Dec. 2012.

[12] H. Rohling, K. Brüninghaus, and R. Grünheid, *Comparison of Multiple Access Schemes for an OFDM Downlink System*. Boston, MA: Springer US, 1997, pp. 23–30.

[13] D. Kivanc, Guoqing Li, and Hui Liu, "Computationally efficient bandwidth allocation and power control for OFDMA," *IEEE Transactions on Wireless Communications*, vol. 2, no. 6, pp. 1150–1158, Nov 2003.

[14] B. Paul, A. R. Chiriyath, and D. W. Bliss, "Survey of RF communications and sensing convergence research," *IEEE Access*, vol. 5, pp. 252–270, 2017.

[15] D. Pinchon and P. Siohan, "Closed-form expressions of optimal short PR FMT prototype filters," in *Proc. IEEE Global Telecommun. Conf.*, 2011.

[16] A. Sahin, I. Guvenc, and H. Arslan, "A survey on multicarrier communications: Prototype filters, lattice structures, and implementation aspects," *IEEE Commun. Surveys Tuts.*, vol. 16, no. 3, pp. 1312–1338, Third 2014.

[17] D. Roque and C. Siclet, "Performances of weighted cyclic prefix OFDM with low-complexity equalization," *IEEE Commun. Lett.*, vol. 17, no. 3, pp. 439–442, March 2013.

[18] C. R. Berger, B. Demissie, J. Heckenbach, P. Willett, and S. Zhou, "Signal processing for passive radar using OFDM waveforms," *IEEE J. Sel. Top. Signal Process.*, vol. 4, no. 1, pp. 226–238, Feb 2010.

[19] S. Bidon, J.-Y. Tourneret, L. Savy, and F. Le Chevalier, "Bayesian sparse estimation of migrating targets for wideband radar," *IEEE Trans. Aerosp. Electron. Syst.*, vol. 50, no. 2, pp. 871–886, Apr. 2014.

[20] C. P. Robert and G. Casella, *Monte Carlo Statistical Methods*. New York, NY: Springer Science, 2004.

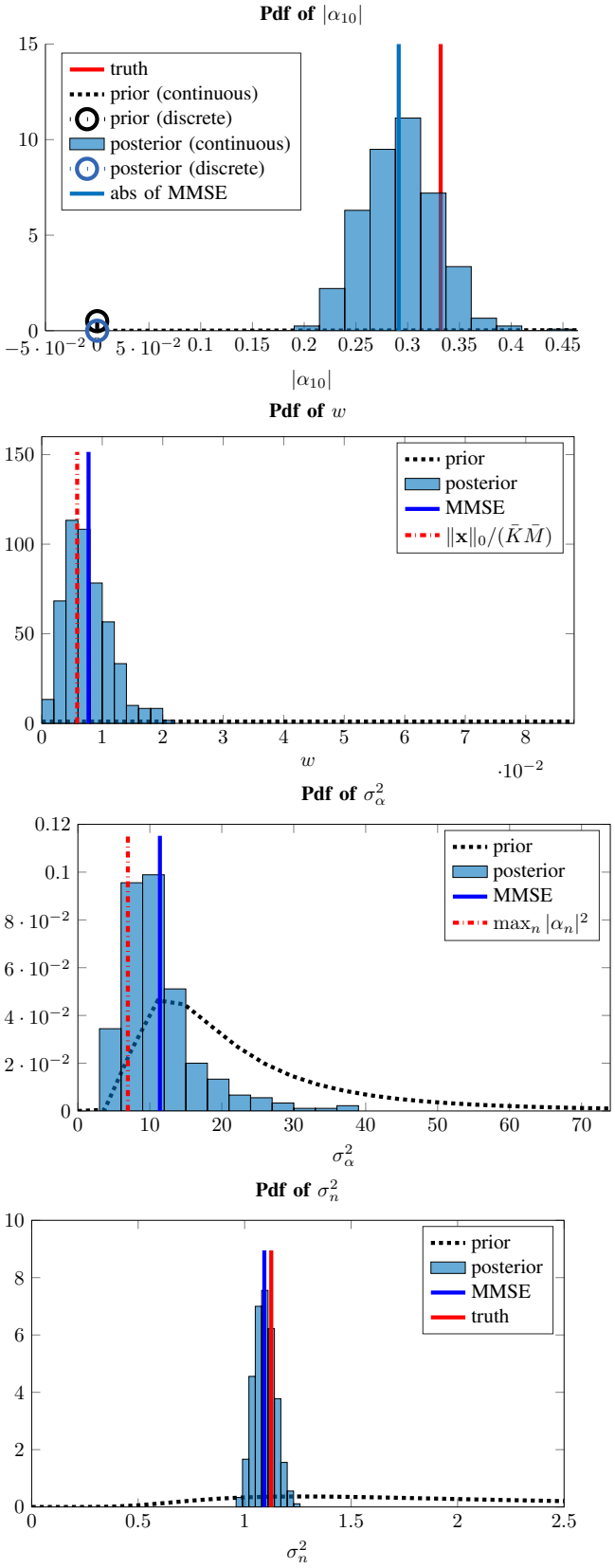

Fig. 4. Empirical posterior pdfs obtained from the proposed SSR-based strategy. Scenario is the same as that of Fig. 3.

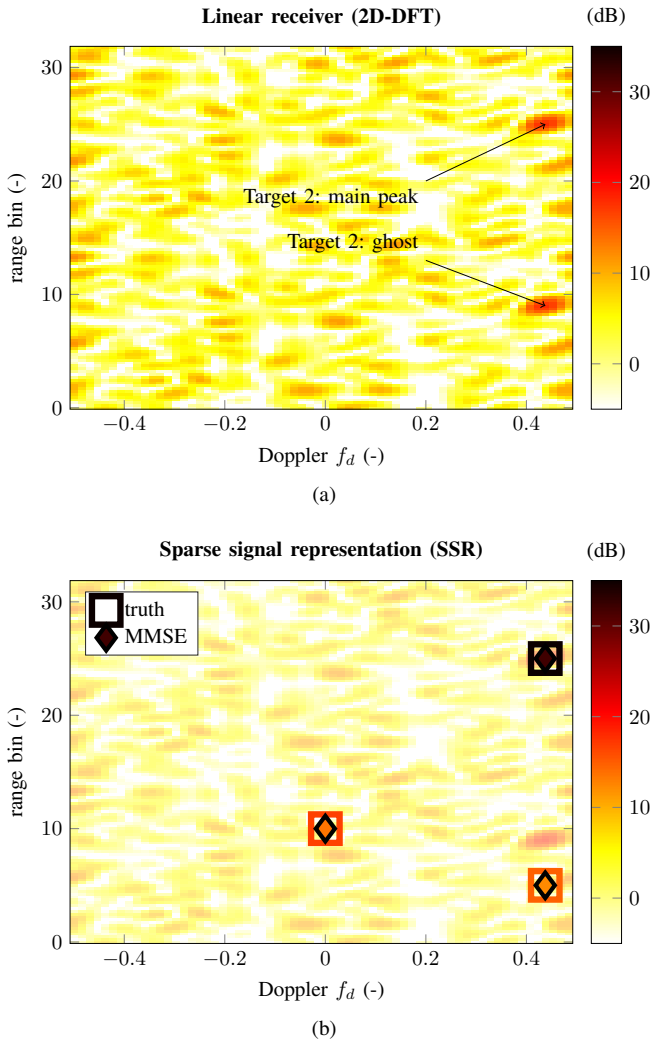

Fig. 5. Range-Doppler map with a CP-OFDM waveform. Scenario is the same as that of Fig. 3 albeit one-in-two subcarriers are used ($K_{\text{user}} = K/2 = 16$). Target SNR in Table I is reduced by a factor $K_{\text{user}}/K = -3$ dB. (a) 2D-DFT output $|\boldsymbol{x}|$ (10). (b) Proposed SSR-based strategy output $K_{\text{user}}KM/(\sigma^2\,\|\check{\boldsymbol{g}}\|_2^2) \times |\hat{\boldsymbol{\alpha}}_{\text{mmse}}|^2$ (2D-DFT output depicted in transparent background as a reference): $\bar{K} = K$, $\bar{M} = M$, $(\beta_0, \beta_1) \approx (3, 50)$, $(\gamma_0, \gamma_1) \approx (2, 4)$, $(N_{bi}, N_r) = (200, 500)$.